SLAC-PUB-12167
October 2006
RBRC-612

Single Transverse-Spin Asymmetries at Large-x

Stanley J. Brodsky[1] and Feng Yuan[2,3]

[1]*Stanford Linear Accelerator Center, Stanford University, Stanford, California 94309*
[2]*RIKEN/BNL Research Center, Building 510A, Brookhaven National Laboratory, Upton, NY 11973*
[3]*Beijing Institute of Modern Physics, Beijing University, Beijing 100871, People's Republic of China*

Abstract

The large-x behavior of the transverse-momentum dependent quark distributions is analyzed in the factorization-inspired perturbative QCD framework, particularly for the naive time-reversal-odd quark Sivers function which is responsible for the single transverse-spin asymmetries in various semi-inclusive hard processes. By examining the dominant hard gluon exchange Feynman diagrams, and using the resulting power counting rule, we find that the Sivers function has power behavior $(1-x)^4$ at $x \to 1$, which is one power of $(1-x)$ suppressed relative to the unpolarized quark distribution. These power-counting results provide important guidelines for the parameterization of quark distributions and quark-gluon correlations.

Submitted to Physical Review D

Work supported in part by Department of Energy contract DE-AC02-76SF00515

I. INTRODUCTION

Single transverse-spin asymmetries (SSA) have a long history, starting from the observation of large SSAs in hadron production in nucleon-nucleon scattering in late 70s and 80s [1]. Since initial or final state phases are required to produce these $T-odd$ observables, SSAs provide a unique window into quantum chromodynamics (QCD) at the amplitude level as well as the role of quark orbital angular momentum in the wave functions of hadrons. Recent experimental observations of sizeable SSAs in hard scattering reactions such as single-inclusive deep inelastic scattering $\ell p \to \ell' \pi^+ X$ have greatly motivated new studies of the underlying mechanisms in QCD. These experiments include semi-inclusive deep inelastic scattering at HERMES at DESY [2], COMPASS at CERN [3], and Jlab [4], and hadron production in nucleon-nucleon scattering at RHIC [5–7]. Large SSAs have been observed in semi-inclusive production of hadrons in DIS for transversely polarized proton target at HERMES [2], and single inclusive hadron production in the forward direction in polarized proton-proton scattering at RHIC [5, 7].

On the theory side, two mechanisms have been proposed in the QCD framework to explain these large SSAs in hard scattering processes. One is based on the QCD collinear factorization where the asymmetries arise from the higher-twist quark-gluon correlation effects (Efremov-Teryev-Qiu-Sterman mechanism) [8, 9]. Another approach explicitly takes into account the effects coming from the intrinsic transverse momentum of partons in hadrons. For example, the Sivers function was proposed in [10] to explain the SSA phenomena in hadronic reactions, where intrinsic transverse momentum plays an important role.

In the last few years, there has been an intensive theoretical development of transverse momentum dependent (TMD) parton distributions and their roles in semi-inclusive processes such as semi-inclusive deep inelastic scattering (SIDIS) and the small transverse momentum Drell-Yan process. The gauge-invariant properties[11–14] of the TMD parton distributions and the relevant factorization formalism [15–18] have been studied thoroughly. For example, the Sivers effect in SIDIS has been shown to arise from the interference of amplitudes differing by one unit of quark orbital angular momentum and the fact that these amplitudes have different final-state phases [11]. The phases arise from the Wilson-line associated with the struck quark as required by gauge invariance [12]. The SSA reverses sign in Drell-Yan reactions because the phases in the Drell-Yan reaction arises from initial-state rather than final-state interactions [11, 12]. Remarkably, the SSA effect in these reactions is leading twist; i.e., it survives in the Bjorken-scaling limit. Moreover, it was recently shown that the above two mechanisms for SSAs are unified for physical processes in the kinematical region where both apply [19].

There has also been a number of phenomenological studies of the experimental data. Model-dependent parameterizations of the relevant non-perturbative parton distributions (twist-3 quark-gluon correlation or the TMD quark distributions) have been adopted to fit to the data [9, 20–23]. In these studies it has been implicitly assumed the Sivers function is suppressed at large x relative to the unpolarized quark distributions [21, 22]. In this paper, we will provide an argument for this suppression based on power-counting of the leading diagrams in perturbative QCD. We will utilize the generalized power counting rule and adopt a perturbative analysis of the structure function at large x.

The large-x behavior of both the polarized and unpolarized parton distributions have been studied [24–28] in PQCD. A generic factorization has recently been used to justify the power counting rule by relating parton distributions at large-x to the quark distribution

amplitudes of hadrons [29]. So far, the power counting results have been worked out for the unpolarized and longitudinal polarized quark distributions. In the present study, we will extend this analysis to other leading-order TMD quark distributions, including the naive time-reversal-odd quark Sivers function which is responsible for the SSAs in various semi-inclusive hard processes.

It is important to note that the $x \to 1$ regime where the struck quark has nearly all of the light-cone momentum of its parent hadron involves dynamics far-off the mass shell: the Feynman virtuality of the struck quark becomes highly space-like: $k_F^2 - m^2 \sim -\frac{k_\perp^2 + \mathcal{M}^2}{1-x}$, where $k_\perp$ and $\mathcal{M}$ are the transverse momentum and invariant mass of the spectator system. Thus we can use perturbative QCD to analyze the large-x behavior of parton distributions since the internal propagators in the relevant Feynman diagrams scale as $1/(1-x)$. This behavior leads to a power counting rule. This is because more partons in hadron's wave function means more propagators in the scattering amplitudes, and more suppression for the contribution to the parton distributions. Thus the parton distributions at large-x depend on the number of partons in the Fock state wave function of the hadron. In particular, the valence Fock state with the minimum number of constituents will dominate the quark distribution function at large-x. For example, the proton structure function will be dominated by its three-quark Fock states, which can be further classified according to its quark orbital angular momentum projection: $L_z = 0$, $|L_z| = 1$, or $|L_z| = 2$ [30]. Since nonzero quark orbital angular momentum light-cone wave function normally introduces additional suppression of $(1-x)$, we will consider in this paper only $L_z = 0$ and $|L_z| = 1$ Fock states contributions. The $|L_z| = 1$ state is needed because some of the TMD quark distributions involve the interference between $L_z = 0$ and $L_z = 1$ states [11, 30, 31] (see also the discussions below).

As is the case of the nucleon form factors (Dirac and Pauli form factors) [32], the transverse momentum dependent quark distributions can be calculated from the overlap of the light-cone wave functions of three-quark Fock states [11, 30, 31]. As we shall demonstrate, the large-x power counting for the TMD parton distributions can be obtained in a similar manner. For example, we know that the unpolarized quark distribution has power counting of $(1-x)^3$ at large-x [24], which comes from the quark orbital angular momentum projection $L_z = 0$ Fock states contribution, whereas the contribution from the overlap of two light-cone functions for $|L_z| = 1$ states is suppressed by $(1-x)^2$[25–28]. On the other hand, since the Sivers function depends on the interference between $L_z = 0$ and $|L_z| = 1$ states, simple counting suggests that that the Sivers function will have the leading power of $(1-x)^4$. The detailed calculations in this paper support this intuitive argument.

The remainder of the paper is organized as follows. In Sec. II, we present our analysis of the leading-order TMD quark distributions at large-x, where we discuss the power counting results for the $k_\perp$-even, $k_\perp$-odd, and naive time-reversal-odd quark distributions respectively. We will also derive the power counting results for the integrated parton distributions at leading-twist and sub-leading-twist. We summarize our results in Sec.III.

II. TRANSVERSE-MOMENTUM DEPENDENT QUARK DISTRIBUTIONS AT LARGE-X

The TMD quark distributions can be defined through the following matrix:

$$\mathcal{M}^{\alpha\beta} \;=\; P^+ \int \frac{d\xi^- d^2\xi_\perp}{(2\pi)^3} e^{-ix\xi^- P^+ + i\xi_\perp \cdot k_\perp} \left\langle PS \left| \overline{\Psi}_v^\beta(\xi) \Psi_v^\alpha(0) \right| PS \right\rangle \;, \tag{1}$$

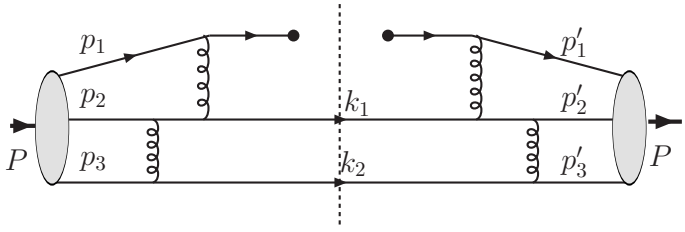

FIG. 1: *Typical Feynman diagram contributing to the large-x quark distribution in nucleon. The blobs at the left and right sides represent the three-quark light-cone wave function distribution amplitudes of the nucleon.*

where the vector $P = (P^+, 0^-, 0_\perp)$ is along the momentum direction of the proton, S is the polarization vector, and $\Psi_v(\xi)$ is defined as

$$\Psi_v(\xi) \equiv \mathcal{L}_v(\infty;\xi)\psi(\xi) \ , \tag{2}$$

with the gauge link $\mathcal{L}_v(\infty;\xi) \equiv \exp\left(-ig\int_0^\infty d\lambda\, v\cdot A(\lambda v+\xi)\right)$. In this paper, we will study the TMD quark distributions for the semi-inclusive DIS processes, thus the above gauge link goes to $+\infty$. Our results can be simply extended to the TMD quark distributions for the Drell-Yan process, where the naive time-reversal-odd TMDs will have an opposite sign [11–13]. In the following analysis, no light-cone singularity will be present, thus we can choose the vector v to be a light-cone vector $n = (0^+, n^-, 0_\perp)$ with $n\cdot P = 1$.

The leading order expansion of the matrix $\mathcal{M}$ contains eight quark distributions [33]. Among the eight distributions, three are the so-called $k_\perp$-even TMD quark distributions: $q(x,k_\perp)$, $\Delta q_L(x,k_\perp)$, and $\delta q_T(x,k_\perp)$, which correspond to the unpolarized, longitudinal polarized, and transversity distributions, respectively. These distributions will lead to the three leading-twist integrated quark distributions [34] after integrating over transverse momentum. The other five distributions are $k_\perp$-odd, and vanish when $k_\perp$ are integrated. Two of them, $q_T(x,k_\perp)$ (Sivers) and $\delta q(x,k_\perp)$ (Boer-Mulders), are odd under naive time-reversal transformation [35]. The notations for these distributions follow Ref. [30], which are different than those in [33]. However, their definitions are identical.

In this paper we are interested in studying the large-x behavior of these TMD quark distributions. We will disregard the $k_\perp$ dependence, and further choose $k_\perp \gg \Lambda_{\rm QCD}$ in order to avoid the infrared divergence associated with low transverse momentum limit. A typical Feynman diagram contributing to large-x quark distributions is shown in Fig. 1. At this order, we can write down an inspired factorization formula for the the parton distributions in terms of the distribution amplitudes of the nucleon [25, 26],

$$\begin{aligned} f(x,k_\perp) \ = \ & \int \frac{d^2k_{1\perp}d^2k_{2\perp}}{4(2\pi)^6}\frac{dz_1dz_2}{z_1z_2}\delta(k_\perp+k_{1\perp}+k_{2\perp})\delta(z_1+z_2+x-1)\int [dy_i][dy_i'] \\ & \Phi(y_i)\Phi'(y_i')\mathcal{H}(y_i,y_i';k_{i\perp};z_i) \ , \end{aligned} \tag{3}$$

where the outside integral represents the phase space integrals for the final state two quarks going through the cut line, with momenta: $k_i = (z_iP^+, k_i^-, k_{i\perp})$ $(i=1,2)$. The inside integral measure $[dy_i]$ is defined as $[dy_i] = dy_1dy_2dy_3\delta(1-y_1-y_2-y_3)$, and the y_i are the momentum fractions of the proton carried by the quarks in the light cone wave functions, i.e., $p_i = y_iP$ and $p_i' = y_i'P$ in Fig. 1. Here f represents any of the leading order TMD quark distributions. Φ and Φ' represent the quark distribution amplitudes of nucleon at the left

and right sides of the cut line, respectively. They can be the leading-twist or higher-twist distribution amplitudes, depending on the quark orbital angular momentum projection along z-direction. We list the distribution amplitudes we will use in this paper in the Appendix for reference. $\mathcal{H}$ represents the hard part which can be calculated from the perturbative Feynman diagram like Fig. 1.

We notice that, in the above equation the phase space integral for k_1 and k_2 are strongly constrained in the limit of $x \to 1$, because of momentum conservation, $z_1 + z_2 = 1 - x$. We can factor out the $(1-x)$ dependence of this phase space integral, taking the following parameterizations: $z_1 = \alpha(1-x),\ z_2 = \beta(1-x)$,

$$\int \frac{dz_1 dz_2}{z_1 z_2} \delta(z_1 + z_2 + x - 1) = \frac{1}{1-x} \int \frac{d\alpha d\beta}{\alpha\beta} \delta(1 - \alpha - \beta) \ . \tag{4}$$

This leads to an overall enhancement of $1/(1-x)$. After factoring this out, the remaining measure of the phase space integral $(d\alpha d\beta)$ does not contain any additional factors of $(1-x)$.

Additional $(1-x)$ factors can come from the hard amplitude $\mathcal{H}$, but these depend on the structure of the relevant tree diagrams. Since the hard propagators each contain a $(1-x)$ factor, the least number of active particles involved in the hard process lead to the least suppression. Thus the leading contribution to the quark distributions at large-x is dominated by the leading component in the hadron's Fock state expansion. For the nucleon, the three-quark Fock state components will dominate the quark distributions, while for pion it will be the quark-antiquark pair states. In the following we will study the large-x power counting for the above mentioned TMD quark distributions, including the three $k_\perp$-even ones: q, Δq_L, δq_T, and four $k_\perp$-odd ones: δq_L, Δq_T, q_T, and δq. For $\delta q'_T$, its analysis will involve much more complicated diagrams, and we will not discussed this in the present paper.

A. $k_\perp$-even quark distributions

The unpolarized quark distribution is defined as

$$q(x, k_\perp) = \frac{1}{2} \int \frac{d\xi^- d^2\xi_\perp}{(2\pi)^3} e^{-ix\xi^- P^+ + i\xi_\perp \cdot k_\perp} \left\langle P \left| \overline{\Psi}_v(\xi) \gamma^+ \Psi_v(0) \right| P \right\rangle \ . \tag{5}$$

The large-x power counting for this distribution function has been studied in the literature [24, 25]. In the following, we will repeat these arguments as guideline for the analysis of other quark distributions.

We calculate the above matrix element in the proton helicity basis,

$$q(x, k_\perp) = \frac{1}{2} \int \frac{d\xi^- d^2\xi_\perp}{(2\pi)^3} e^{-ix\xi^- P^+ + i\xi_\perp \cdot k_\perp} \frac{1}{2} \left(\langle PS_{z\uparrow} | \hat{\mathcal{O}} | PS_{z\uparrow} \rangle + \langle PS_{z\downarrow} | \hat{\mathcal{O}} | PS_{z\downarrow} \rangle \right) \ , \tag{6}$$

where the operator $\hat{\mathcal{O}}$ is defined as $\hat{\mathcal{O}} = \overline{\Psi}_v(\xi)\gamma^+\Psi_v(0)$. This operator is chiral-even, and conserves the quark helicity in the partonic scattering matrix elements, and so that the dominant contributions come from the leading Fock state wave function ($L_z = 0$) at both sides of the cut in Fig. 1. The matrix element $\langle PS_{z\uparrow} | \hat{\mathcal{O}} | PS_{z\uparrow} \rangle$ will have the contributions from the following quark spin configurations: $\uparrow\downarrow\uparrow$ and $\downarrow\uparrow\uparrow$, where in the first one the probing quark has the same helicity as the proton and in the second case it is opposite. If the probing quark's spin is parallel to the proton spin, the two spectator quarks will form a scalar.

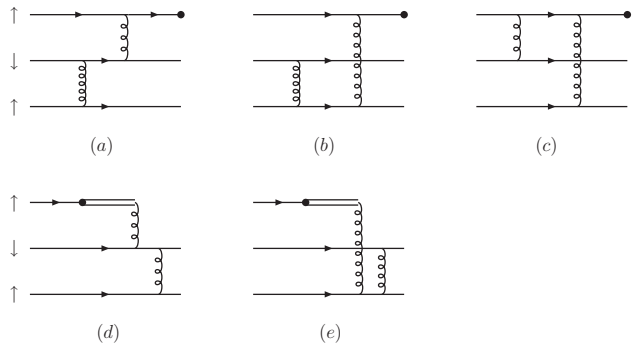

FIG. 2: *Leading diagrams contributing to the $k_\perp$-even quark distributions at large-x: left half of the relevant diagrams are shown. The contributions will the amplitudes square of these diagrams, including the interference between them. These diagrams also contribute to the $k_\perp$-odd and naive time-reversal-odd TMD quark distributions.*

In the following, we are only interested in obtaining the power counting for the quark distributions, and the explicit dependence on the distribution amplitudes will not be discussed. According to the factorization formula Eq. (3) and the reduced integral Eq. (4), the unpolarized quark distribution depends on the leading-twist distribution amplitudes of the nucleon,

$$q(x,k_\perp)|_{x\to 1} \propto \frac{1}{1-x}\int \frac{d\alpha d\beta}{\alpha\beta}\Phi_3(y_i)\Phi_3(y_i')\mathcal{H}\left(y_i;y_i';\alpha,\beta,(1-x)\right) \ . \tag{7}$$

The power counting of the hard factor $\mathcal{H}$ can be evaluated from the partonic scattering matrix elements, which include a set of propagators and traces of the Dirac matrices. As mentioned above, the propagators are far off-shell in the limit of $x \to 1$, which will lead to suppression in terms of $(1-x)$. For example, One of the gluon propagator in Fig. 1 goes like,

$$\frac{1}{(p_3-k_2)^2} = \frac{1}{2p_3\cdot k_2} \approx -\frac{1}{\langle k_\perp^2\rangle}\frac{1-x}{y_3} \ , \tag{8}$$

at large x. In the above expression, we have omitted all higher order terms suppressed by $(1-x)$. $\langle k_\perp^2\rangle$ represents a typical momentum scale in order of transverse momentum $k_\perp$. Besides the propagators, the traces of the Dirac matrix contains $(1-x)$ factors as well, which will depend on the spin structure of the quarks in the scattering matrix elements. For example, the traces of the Dirac matrices for the scattering $\uparrow\downarrow\uparrow\to\uparrow\downarrow\uparrow$ in Fig. 1 will contribute to the matrix element $\langle PS_{z\uparrow}|\hat{\mathcal{O}}|PS_{z\uparrow}\rangle$ as

$$\frac{1}{(1-x)^4} \ , \tag{9}$$

in the leading power, where the probing quark has the same helicity as the proton. If the probing quark has an opposite helicity as the proton, e.g., in the spin structure $\downarrow\uparrow\uparrow$, the Dirac trace for the diagram of Fig. 1 vanishes. We have checked all other diagrams, and found that the Dirac traces for those diagrams with spin-one configuration for the spectator quarks ($\uparrow\uparrow$ or $\downarrow\downarrow$ for the two spectator quarks) either vanish or are suppressed by at least $(1-x)^2$ as compared to the scalar configuration ($\uparrow\downarrow$ or $\downarrow\uparrow$). This property has long been noticed in the literature [24, 25, 27]. In Fig. 2, we showed all leading diagrams for the spin structure of $\uparrow\downarrow\uparrow$, where only left half sides of the relevant diagrams are shown. The contributions will be the amplitudes square of these diagrams, including their interferences.

In summary, the leading contribution to the matrix element in Eq. (6) comes from the quark spin structure with probing quark's helicity equal to the nucleon's helicity. If they differ, the contribution will be suppressed by $(1-x)^2$. This is to say, the quark distribution is dominated by the quark spin parallel to the nucleon spin, and the quark spin anti-parallel distribution will be suppressed by $(1-x)^2$.

The final power counting result will depend on the above factors, including the Dirac matrix traces, the power counting of the propagators, and the phase spaces integrals. For example, the diagram in Fig. 1 contains eight propagators, with overall power counting,

$$\sim \frac{(1-x)^8}{y_3(1-y_1)^2 y_3'(1-y_1')^2} \ . \tag{10}$$

Combining the above with the contribution from the Dirac matrix traces in Eq. (9) and the phase spaces integral factor in Eq. (4), we find that the contribution of this diagram to the unpolarized quark distribution is

$$q(x,k_\perp)|_{x\to 1} \sim (1-x)^3 \ . \tag{11}$$

All other diagrams in Fig. 2 will contribute the same power to the unpolarized quark distribution. For example, the amplitude square of Fig. 2(d) contribute a power of $(1-x)^{-2}$ from the Dirac matrix traces, a power of $(1-x)^6$ from the propagators, plus a power of $(1-x)^{-1}$ from the phase space integral Eq. (4), which leads to a power of $(1-x)^3$ contribution to the quark distribution.

The longitudinal polarized quark distribution can be analyzed accordingly, which is defined through the following matrix element,

$$\Delta q_L(x,k_\perp) = \frac{1}{2}\int \frac{d\xi^- d^2\xi_\perp}{(2\pi)^3} e^{-ix\xi^- P^+ + i\xi_\perp\cdot k_\perp} \left\langle PS_z \left| \overline{\Psi}_v(\xi)\gamma^+\gamma_5\Psi_v(0)\right| PS_z\right\rangle \ . \tag{12}$$

Again, if we calculate in the proton helicity states, we will obtain

$$\Delta q_L(x,k_\perp) = \frac{1}{2}\int \frac{d\xi^- d^2\xi_\perp}{(2\pi)^3} e^{-ix\xi^- P^+ + i\xi_\perp\cdot k_\perp} \frac{1}{2}\left(\langle PS_{z\uparrow}|\hat{\mathcal{O}}_L|PS_{z\uparrow}\rangle - \langle PS_{z\downarrow}|\hat{\mathcal{O}}_L|PS_{z\downarrow}\rangle\right) \ , \tag{13}$$

where the operator $\hat{\mathcal{O}}_L$ is defined as $\hat{\mathcal{O}}_L = \overline{\Psi}_v(\xi)\gamma^+\gamma_5\Psi_v(0)$. We can interpret longitudinal polarized quark distribution as the quark spin parallel to the nucleon spin distribution minus the antiparallel distribution. According to the above analysis for the unpolarized quark distribution, we know that the quark spin parallel to the nucleon spin distribution dominates over the antiparallel distribution, and the latter is suppressed by an extra factor of $(1-x)^2$. In conclusion, we will obtain the same power behavior for the longitudinal polarized quark distribution as the unpolarized quark distribution,

$$\Delta q_L(x,k_\perp)|_{x\to 1} \sim (1-x)^3 \ . \tag{14}$$

The transversity distribution for the quarks can be analyzed in the same way. It is defined as

$$\delta q_T(x,k_\perp) = \frac{1}{2}\int \frac{d\xi^- d^2\xi_\perp}{(2\pi)^3} e^{-ix\xi^- P^+ + i\xi_\perp\cdot k_\perp} \langle PS_\perp|\overline{\Psi}_v(\xi)\gamma^+\gamma^\perp\gamma_5\Psi_v(0)|PS_\perp\rangle \ . \tag{15}$$

Here, the proton is transversely polarized. We can choose the polarization vector along x-direction, and the polarization states can be constructed from the proton helicity states,

$$|PS_{x\uparrow}\rangle = \frac{1}{\sqrt{2}}\left(|PS_{z\uparrow}\rangle + |PS_{z\downarrow}\rangle\right) \ , \quad |PS_{x\downarrow}\rangle = \frac{1}{\sqrt{2}}\left(|PS_{z\uparrow}\rangle - |PS_{z\downarrow}\rangle\right) \ . \tag{16}$$

Substituting the above into the definition of the transversity distribution, we will obtain

$$\delta q_T(x,k_\perp) = \frac{1}{2}\int \frac{d\xi^- d^2\xi_\perp}{(2\pi)^3} e^{-ix\xi^- P^+ + i\xi_\perp\cdot k_\perp} \frac{1}{2}\left(\left\langle PS_{z\uparrow}|\hat{\mathcal{O}}_t|PS_{z\downarrow}\right\rangle + \left\langle PS_{z\downarrow}\left|\hat{\mathcal{O}}_t\right|PS_{z\uparrow}\right\rangle\right) \ , \tag{17}$$

where the operator $\hat{\mathcal{O}}_t$ is defined as $\hat{\mathcal{O}}_t = \overline{\Psi}_v(\xi^-,0,\vec{b}_\perp)\gamma^+\gamma^\perp\gamma_5\Psi_v(0)$. From this equation, we see that the quark transversity distribution depends on the matrix elements with hadron helicity flip. On the other hand, because the operator $\hat{\mathcal{O}}_t$ is chiral-odd, it changes the quark helicity in the partonic scattering process as well. If we keep the leading Fock state contribution, the matrix element in the bracket of the above equation will reduce to

$$_{\frac{1}{2}}\left\langle PS_{z\uparrow}|\hat{\mathcal{O}}_t|PS_{z\downarrow}\right\rangle_{-\frac{1}{2}} + {}_{-\frac{1}{2}}\left\langle PS_{z\downarrow}\left|\hat{\mathcal{O}}_t\right|PS_{z\uparrow}\right\rangle_{\frac{1}{2}} \ , \tag{18}$$

where the subscripts $\pm\frac{1}{2}$ represents the total quark helicity in the three-quark wave function used in the calculations. From this equation, we can easily see that it will be the same set of diagrams in Fig. 2 contributing to the transversity quark distributions. The same power counting results will be obtained,

$$\delta q_T(x,k_\perp)|_{x\to 1} \sim (1-x)^3 \ . \tag{19}$$

From the above analysis, all the three $k_\perp$-even quark distributions have the same power behavior at large-x, which is certainly consistent with the inequality condition for them [36].

B. $k_\perp$-odd and naive time-reversal-even quark distributions

In this subsection, we will study two $k_\perp$-odd but naive time-reversal-even TMD quark distributions: Δq_T and δq_T, which represent the longitudinal polarized quark distribution in a transversely polarized proton and the transversely polarized quark distribution in a longitudinal polarized proton, respectively. Δq_T can be calculated from the following matrix element,

$$\Delta q_T(x,k_\perp) = \frac{M_P}{2S_\perp\cdot k_\perp}\int \frac{d\xi^- d^2\xi_\perp}{(2\pi)^3} e^{-ix\xi^- P^+ + i\xi_\perp\cdot k_\perp}\left\langle PS_\perp|\hat{\mathcal{O}}_L|PS_\perp\right\rangle \ , \tag{20}$$

where the operator $\hat{\mathcal{O}}_L$ as defined above. Following the above calculation for the transversity distribution, we choose the transverse polarization vector along the x-direction, and the above equation can be reduced to

$$\Delta q_T(x,k_\perp) = \frac{M_P}{2k_\perp^x}\int \frac{d\xi^-}{(2\pi)^3} e^{-ix\xi^- P^+ + i\xi_\perp\cdot k_\perp}\frac{1}{2}\left(\left\langle PS_{z\uparrow}|\hat{\mathcal{O}}_L|PS_{z\downarrow}\right\rangle + \left\langle PS_{z\downarrow}\left|\hat{\mathcal{O}}_L\right|PS_{z\uparrow}\right\rangle\right) \ . \tag{21}$$

$\hat{\mathcal{O}}_L$ is a chiral-even operator, and it conserves the quark helicity. On the other hand, the above matrix element has hadron helicity flip, thus the total quark helicity and the hadron

helicity will mismatch on either side of the above matrix element. If the total quark helicity and the proton helicity is mismatching, the wave function for the three-quark state must have nonzero quark orbital angular momentum. It is the interference between the $L_z = 0$ and $|L_z| = 1$ states contributing to the TMD quark distribution Δq_T.

In order to proceed, we further decompose the proton spin state into the Fock states containing $L_z = 0$ and $|L_z| = 1$. For example,

$$|PS_{z\uparrow}\rangle = |PS_{z\uparrow}\rangle_{1/2} + |PS_{z\uparrow}\rangle_{-1/2} \ , \tag{22}$$

where the subscript $\pm 1/2$ denotes the total quark helicity. The first term in the above equation represents the $L_z = 0$ state, while second one for the $L_z = 1$ state. The wave function parameterizations for these states have been given in Eq. (A1). Similarly, for $|PS_{z\downarrow}\rangle$ we have,

$$|PS_{z\downarrow}\rangle = |PS_{z\downarrow}\rangle_{-1/2} + |PS_{z\downarrow}\rangle_{1/2} \ , \tag{23}$$

where the first one is for $L_z = 0$, and the second one for $L_z = -1$. Because the partonic matrix element conserves the quark helicity, in the calculation of the matrix element of Eq. (21), the quarks helicities will remain the same at the left and right sides of the cut line in the Feynman diagram like Fig. 1. From the experience in the last subsection, we know that the partonic processes where the two spectator quarks have opposite helicities dominate the quark distributions at large-x. So, for the leading contributions we will have two typical partonic processes: $\uparrow\downarrow\uparrow\to\uparrow\downarrow\uparrow$ with total quark helicity $1/2$ and $\downarrow\uparrow\downarrow\to\downarrow\uparrow\downarrow$ with total quark helicity $-1/2$. These two actually will contribute opposite sign to the matrix element in Eq. (21), because of the γ_5 in the operator $\hat{\mathcal{O}}_L$. Taking into account this fact, and substituting the above decomposition into Eq. (21), we find that the matrix element becomes

$$\begin{aligned} &{}_{\frac{1}{2}}\langle PS_{z\uparrow}|\hat{\mathcal{O}}_L|PS_{z\downarrow}\rangle_{\frac{1}{2}} \ - \ {}_{-\frac{1}{2}}\langle PS_{z\downarrow}|\hat{\mathcal{O}}_L|PS_{z\uparrow}\rangle_{-\frac{1}{2}} \\ -{}_{-\frac{1}{2}}&\langle PS_{z\uparrow}|\hat{\mathcal{O}}_L|PS_{z\downarrow}\rangle_{-\frac{1}{2}} \ + \ {}_{\frac{1}{2}}\langle PS_{z\downarrow}|\hat{\mathcal{O}}_L|PS_{z\uparrow}\rangle_{\frac{1}{2}} \ . \end{aligned} \tag{24}$$

It is easy to see that the above two lines are complex conjugates. In the following, we will consider the contribution from the first line, and the other one can be obtained immediately.

For the subprocess $\uparrow\downarrow\uparrow\to\uparrow\downarrow\uparrow$, the contribution to the matrix element will be

$${}_{\frac{1}{2}}\langle PS_{x\uparrow}|\hat{\mathcal{O}}|PS_{x\downarrow}\rangle_{\frac{1}{2}} \propto \int \tilde{\psi}^{(1)}(y_i')\tilde{\psi}^{(3)}(y_i, p_{i\perp})\,(p_1^x - ip_1^y)\,T_H(y_i; y_i'; p_{i\perp}) \ , \tag{25}$$

where $\tilde{\psi}^{(1)}$ is the wave function for $L_z = 0$ Fock state and $\tilde{\psi}^{(3)}$ for $|L_z| = 1$ (their definitions are listed in the Appendix). Here we only show the contribution from the interference between $\tilde{\psi}^{(1)}$ and $\tilde{\psi}^{(3)}$ wave functions, and other interference contributions (e.g., the one with $\tilde{\psi}^{(1)}$ and $\tilde{\psi}^{(4)}$) can be calculated similarly. Because proton is stable, the light-cone wave functions are real, i.e., $(\tilde{\psi})^* = \tilde{\psi}$. Meanwhile, for the $\downarrow\uparrow\downarrow\to\downarrow\uparrow\downarrow$ partonic process, we will have

$${}_{-\frac{1}{2}}\langle PS_{x\downarrow}|\hat{\mathcal{O}}|PS_{x\uparrow}\rangle_{-\frac{1}{2}} \propto \int \tilde{\psi}^{(1)}(y_i')\tilde{\psi}^{(3)}(y_i, p_{i\perp})\,(-p_1^x - ip_1^y)\,T_H(y_i; y_i'; p_{i\perp}) \ . \tag{26}$$

The hard partonic parts T_H in the above two equations are identical to each other for the same diagram if we change all the quarks helicities. Thus we can sum their contributions together, and the matrix element will be

$$\langle PS_{x\uparrow}|\hat{\mathcal{O}}|PS_{x\downarrow}\rangle - \langle PS_{x\downarrow}|\hat{\mathcal{O}}|PS_{x\uparrow}\rangle \propto \int \tilde{\psi}^{(1)}(y_i')\tilde{\psi}^{(3)}(y_i, p_{i\perp})\,(p_1^x)\,T_H(y_i; y_i'; p_{i\perp}) + h.c. \tag{27}$$

The linear expansion term of $p_{i\perp}$ from T_H will be crucial to obtain nonzero contribution to the above matrix element when integrating over $p_{i\perp}$. Otherwise, it will vanish. This expansion will introduce an additional suppression factor in $(1-x)$. For example, one of the propagators in Fig. 1 has the following expansion result,

$$\begin{aligned}\frac{1}{(p_3-k_2)^2} &= \frac{1}{(y_3P-k_2+p_{3\perp})^2} \\ &= \frac{\beta(1-x)}{y_3k_{2\perp}^2}\left(1-\frac{\beta(1-x)}{y_3k_{2\perp}^2}2p_{3\perp}\cdot k_{2\perp}\right) \ . \end{aligned} \tag{28}$$

Substituting the above into Eq. (27), and using the fact that $p_{3\perp}=-p_{1\perp}-p_{2\perp}$, we find that the above expansion will lead to a contribution as $(1-x)\int d^2p_{1\perp}p_{1\perp}^x\,(p_{1\perp}\cdot k_\perp)\,\tilde{\psi}^{(3)} \sim (1-x)k_\perp^x\Phi^{(3,4)}$, where $\Phi^{(34)}$ represents a combination of twist-four distribution amplitudes Φ_4 and Ψ_4, and the $k_\perp^x$ factor will cancel out the same $k_\perp^x$ in the denominator in Eq. (21). This suppression feature applies to every propagator expansion containing the linear term of the intrinsic transverse momentum $p_\perp$. Similarly, the Dirac wave function expansion in terms of $p_\perp$ will also be suppressed by $(1-x)$.

The above analysis can be repeated for every diagrams in Fig. 2, and they contribute the same. So, the final power counting result for the TMD quark distribution Δq_T will be,

$$\Delta q_T(x,k_\perp)|_{x\to 1} \sim (1-x)^4 \ . \tag{29}$$

Similar analysis can be performed for the TMD quark distribution δq_L, which is defined through the following matrix element,

$$\delta q_L(x,k_\perp) = \frac{M_P}{2k_\perp^i}\int\frac{d\xi^-d^2\xi_\perp}{(2\pi)^3}e^{-ix\xi^-P^+ + i\xi_\perp\cdot k_\perp}\left\langle PS_z|\overline{\Psi}_v(\xi)\gamma^+\gamma^i\gamma_5\Psi_v(0)|PS_z\right\rangle \ . \tag{30}$$

If we choose $\gamma^i=\gamma^x$ in the above equation, the TMD δq_L will become,

$$\delta q_L(x,k_\perp) = \frac{M_P}{2k_\perp^x}\int\frac{d\xi^-d^2\xi_\perp}{(2\pi)^3}e^{-ix\xi^-P^+ + i\xi_\perp\cdot k_\perp}\langle PS_z|\hat{\mathcal{O}}_t|PS_z\rangle \ , \tag{31}$$

where the operator $\hat{\mathcal{O}}_t$ follows the definition in the subsection Sec.II(b). In the above definition, the proton is longitudinal polarized, and we can further write down explicitly in terms of the proton helicity states,

$$\delta q_L(x,k_\perp) = \frac{M_P}{2k_\perp^x}\int\frac{d\xi^-d^2\xi_\perp}{(2\pi)^3}e^{-ix\xi^-P^+ + i\xi_\perp\cdot k_\perp}\frac{1}{2}\left(\langle PS_{z\uparrow}|\hat{\mathcal{O}}_t|PS_{z\uparrow}\rangle - \langle PS_{z\downarrow}|\hat{\mathcal{O}}_t|PS_{z\downarrow}\rangle\right) \ . \tag{32}$$

Since the operator $\hat{\mathcal{O}}_t$ is chiral-odd, it changes the quark helicity. However, in the above equation, we are calculating the hadron helicity conserved matrix elements, thus the nonzero quark orbital angular momentum projection must be taken into account in order to obtain nonzero results, as in the case of Δq_T in the above. Following the above analysis, we find the power counting result for the TMD quark distribution δq_L,

$$\delta q_L|_{x\to 1} \sim (1-x)^4 \ , \tag{33}$$

which is one power of $(1-x)$ suppressed relative to the unpolarized quark distribution.

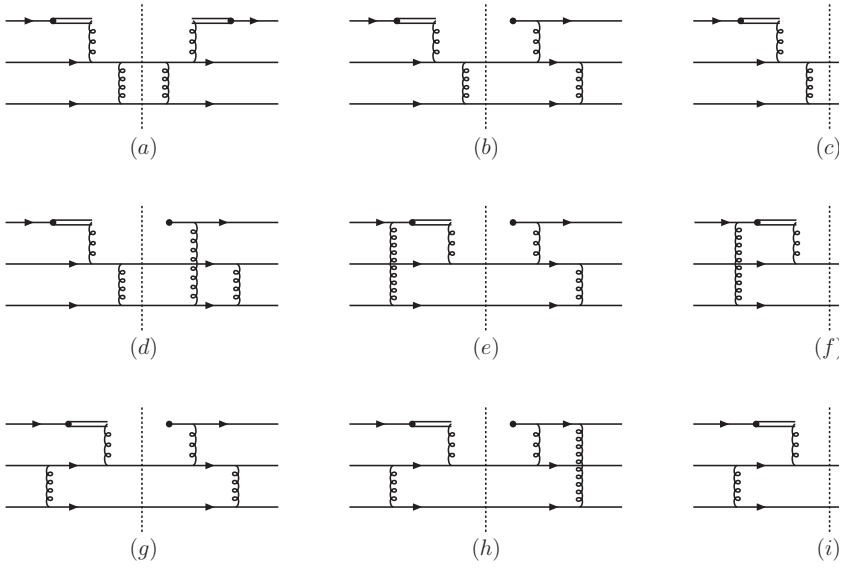

FIG. 3: *Leading Feynman diagrams contributing to the naive time-reversal-odd TMD quark distributions at large-x.*

C. Naive time-reversal-odd quark distributions

Now, we turn to the naive time-reversal-odd quark distributions. At leading order, we have two: the quark Sivers function and the Boer-Mulders function. The Sivers function represents the unpolarized quark distribution in a transversely polarized target, while the Boer-Mulders function represents the transversely polarized quark distribution in a unpolarized proton target. These two distributions are naive time-reversal-odd, and their existence require final state interactions [11]. The quark Sivers function is defined as,

$$q_T(x,k_\perp) = \frac{M}{2\epsilon^{ij}S_\perp^i k_\perp^j}\int \frac{d\xi^- d^2\xi_\perp}{(2\pi)^3} e^{-ix\xi^- P^+ + i\xi_\perp\cdot k_\perp}\langle PS|\hat{\mathcal{O}}|PS\rangle \ , \tag{34}$$

where the operator $\mathcal{O}$ follows the above definition. Because the target is transversely polarized, again we will choose the x-direction for its polarization, and the Sivers function then becomes,

$$q_T(x,k_\perp) = \frac{M}{2k_\perp^y}\int \frac{d\xi^- d^2\xi_\perp}{(2\pi)^3} e^{-ik\cdot\xi}\frac{1}{2}\left(\langle PS_{z\uparrow}|\hat{\mathcal{O}}|PS_{z\downarrow}\rangle + \langle PS_{z\downarrow}|\hat{\mathcal{O}}|PS_{z\uparrow}\rangle\right) \ . \tag{35}$$

The above equation shows that the Sivers function is proportional to the matrix elements involving hadron helicity flip. Because the operator $\hat{\mathcal{O}}$ is chiral-even, it conserves the quark helicities. To obtain the hadron helicity flip, we have to take into account the nucleon's light-cone wave function with nonzero quark orbital angular momentum, as in the previous two examples.

Following the calculations in the last subsection for $k_\perp$-odd distribution Δq_T, we find that the Sivers function will depend on the following matrix element,

$$\begin{aligned} &{}_{\frac{1}{2}}\langle PS_{z\uparrow}|\hat{\mathcal{O}}|PS_{z\downarrow}\rangle_{\frac{1}{2}} \ + \ {}_{-\frac{1}{2}}\langle PS_{z\downarrow}|\hat{\mathcal{O}}|PS_{z\uparrow}\rangle_{-\frac{1}{2}} \\ +{}_{-\frac{1}{2}}&\langle PS_{z\uparrow}|\hat{\mathcal{O}}|PS_{z\downarrow}\rangle_{-\frac{1}{2}} \ + \ {}_{\frac{1}{2}}\langle PS_{z\downarrow}|\hat{\mathcal{O}}|PS_{z\uparrow}\rangle_{\frac{1}{2}} \ . \end{aligned} \tag{36}$$

Comparing with Eq. (24), we find that only the sign changes in the above sum. This is because here we are probing the unpolarized quark, and we have to sum up different quark helicity contribution, while in Eq. (24) we are probing the longitudinal polarized quark and different quark helicity will contribute differently. From Eqs. (25,26), we find that the final result for the above matrix element will be

$$\langle PS_{x\uparrow}|\hat{\mathcal{O}}|PS_{x\downarrow}\rangle + \langle PS_{x\downarrow}|\hat{\mathcal{O}}|PS_{x\uparrow}\rangle \propto \int \tilde{\psi}^{(1)}(y_i')\tilde{\psi}^{(3)}(y_i)\,(-ip_1^y)\,T_H(y_i;y_i';p_{i\perp}) + h.c.\ . \quad (37)$$

From this equation, we find that in order to generate a nonzero Sivers function, the hard scattering factor T_H has to have an imaginary part. In a partonic hard scattering amplitude, the only imaginary part comes from the on-shell pole of some propagator. As we showed in the above analysis all the propagators in Fig. 2 are far off-shell except for the eikonal propagator from the gauge link. Thus, in order to obtain nonzero contribution to the Sivers function, we have to have eikonal propagator in the partonic Feynman diagrams. We have shown all leading order diagrams contribution to the Sivers function in Fig. 3, all of which have at least one eikonal propagator. For example, the eikonal propagator in Fig. 3(a) reads,

$$\frac{1}{n\cdot(k-p_1)+i\epsilon} = P\frac{1}{x-y_1} - i\pi\delta(x-y_1)\ , \quad (38)$$

where the first term is the principal value of the pole, and does not contribute to the Sivers function. Only the second term contribute to an imaginary part, which contains a delta function. This delta function will affect the power counting for the various factors in the evaluation of the matrix element of Eq. (37). This is because the delta function can be written as $\delta(x-y_1) = \delta\left(y_2+y_3-(1-x)\right)$, which means that the variables y_2 and y_3 are limited to be order of $(1-x)$, i.e., $y_2 \sim y_3 \sim \mathcal{O}(1-x)$. All factors which depend on y_2 and y_3 will have to be examined carefully to get the right power counting results. For example, in Fig. 3(a), the propagators at the left side of the cut will be affected by the above constraints. One of the gluon propagator reads,

$$\frac{1}{(p_3-k_2)^2} \approx \frac{1}{-y_3\frac{\vec{k}_{2\perp}^2}{\beta(1-x)}} \approx \frac{1}{\langle k_\perp^2\rangle}\ , \quad (39)$$

because $y_3 \sim \mathcal{O}(1-x)$ and β is order of unit. Unlike the case studied in the above subsections, this propagator does not lead to a suppression in $(1-x)$ for the Sivers function. Similarly, another gluon propagator and the quark propagator at the left side of the cut line are also finite at $x \to 1$. However, all the propagators at the right hand side of the cut line still scale as $(1-x)$, and the total four propagators there will contribute to a suppression factor of $(1-x)^4$.

Another consequence of this delta function is that the intrinsic $p_\perp$ expansion in the hard part has no additional suppression in $(1-x)$, which is very different from what we have in the last subsection for the $k_\perp$-odd but naive time-reversal-even quark distributions. For example, in one of the above propagators, we can keep the intrinsic transverse momentum dependence and expand it up to the linear term,

$$\frac{1}{(p_3-k_2)^2} \approx \frac{1}{-2k_2\cdot p_3} = \frac{1}{-\frac{y_3}{\beta(1-x)}k_{2\perp}^2 - 2k_{2\perp}\cdot p_{3\perp}} \approx -\frac{1}{\langle k_\perp^2\rangle}\left(1-\frac{k_{2\perp}\cdot p_{3\perp}}{\langle k_\perp^2\rangle}\right)\ . \quad (40)$$

The last equation of the above comes from the fact that $y_3 \sim o(1-x)$. After combining this expansion with the light-cone wave function, we get $\int p_{1\perp}^y k_{2\perp} \cdot p_{3\perp} \tilde{\psi}^{(3)} \propto k_\perp^y y_3 \Phi_4(y_i)$ or $y_2 \Psi_4(y_i)$, where the $k_\perp^y$ factor will cancel that in the denominator in Eq. (35).

The final step in this analysis will be to factor out $(1-x)$ from the wave function integral. Because the variables y_2 and y_3 are constrained to be order of $(1-x)$ in the $x \to 1$ limit, we have to examine the wave function integral where the end-point behavior of the light-cone wave function will be important. For example, one contribution in the above analysis is the integral of $y_3 \Phi_4(y_1, y_2, y_3)$. We can factor out the overall dependence on $(1-x)$ from the integral,

$$\int dy_1 dy_2 dy_3 \delta(1-y_1-y_2-y_3)\delta(y_1-x) y_3 \Phi_4(y_1,y_2,y_3)$$
$$= (1-x)^3 \int d\zeta d\zeta' \delta(1-\zeta-\zeta')\zeta'(1-x)\Phi_4(x,\zeta(1-x),\zeta'(1-x))/(1-x)^2 \ , \quad (41)$$

where we have re-parameterized $y_2 = \zeta(1-x)$ and $y_3 = \zeta'(1-x)$. The above integral depends on the end-point behavior of the twist-four distribution amplitudes. As we showed in the Appendix, the twist-four distribution amplitude behaviors as $y_3 \Phi_4(y_1, y_2, y_3) \propto y_1 y_2 y_3$ at the end-point region. From this, we find that

$$\lim_{x\to 1} \frac{\zeta'(1-x)\Phi_4(x,\zeta(1-x),\zeta'(1-x))}{(1-x)^2} = \text{finite} \ . \quad (42)$$

Thus the wave function integral indeed contains a suppression factor $(1-x)^3$. In addition, the Dirac matrix traces will also result into a power dependence on $(1-x)$. This can be calculated straightforwardly, and we find the Dirac traces from Fig. 3(a) contribute to a power term as $(1-x)^{-2}$. By summarizing the power counting results from the above analysis and also taking into account the phase spaces integral factor $(1-x)^{-1}$ in Eq. (4), we find the Sivers function will have the following power behavior,

$$q_T(x,k_\perp)|_{x\to 1} \propto (1-x)^4 \ , \quad (43)$$

which is $(1-x)$ suppressed relative to the unpolarized quark distribution. Similar calculations can be performed for all other diagrams in Fig. 3, and they all contribute to a power behavior of $(1-x)^4$ for the quark Sivers function.

The same analysis can be performed for another naive time-reversal odd distribution, the so-called Boer-Mulders function δq, which is defined as

$$\delta q = \frac{M_P}{2\epsilon^{ij}k_\perp^j} \int \frac{d\xi^-}{(2\pi)^3} e^{-ix\xi^- P^+ + i\xi_\perp \cdot k_\perp} \left\langle P|\overline{\Psi}_v(\xi)\gamma^+\gamma^i\gamma_5\Psi_v(0)|P\right\rangle \ . \quad (44)$$

If we choose $\gamma^i = \gamma^x$ in the above equation, the TMD δq will become,

$$\delta q(x,k_\perp) = \frac{M_P}{2k_\perp^y} \int \frac{d\xi^-}{(2\pi)^3} e^{-ix\xi^- P^+ + i\xi_\perp \cdot k_\perp} \langle P|\hat{\mathcal{O}}_t|P\rangle \ , \quad (45)$$

where the operator $\hat{\mathcal{O}}_t$ follows the definition in the above. Unlike the TMD quark distribution δq_L, in the above definition the proton is unpolarized. Thus the explicit expression for δq in the proton helicity states is

$$\delta q(x,k_\perp) = \frac{M_P}{2k_\perp^x} \int \frac{d\xi^-}{(2\pi)^3} e^{-ix\xi^- P^+ + i\xi_\perp \cdot k_\perp} \frac{1}{2}\left(\langle PS_{z\uparrow}|\hat{\mathcal{O}}_t|PS_{z\uparrow}\rangle + \langle PS_{z\downarrow}|\hat{\mathcal{O}}_t|PS_{z\downarrow}\rangle\right) \ . \quad (46)$$

Comparing this expression to Eq. (32) in the last subsection, we find that δq depends on the sum of the two matrix elements, whereas for δq_L it is the difference. As in the analysis for the Sivers function, we find that we need an imaginary part from the hard part, and the same set of diagrams in Fig. 3 contribute. The final result for its power counting will be

$$\delta q|_{x\to 1} \sim (1-x)^4 \ , \tag{47}$$

which is again one power of $(1-x)$ suppressed relative to the unpolarized quark distribution.

D. Comparison with the Power Counting for the GPD E

Summarizing the results in the last two subsections, we find that the $k_\perp$-odd TMD quark distributions are suppressed by a relative factor $(1-x)$ to the $k_\perp$-even ones (e.g., the unpolarized quark distributions). As we mentioned in the introduction, this can also be understood by the interpretation of these TMD quark distributions in terms of the overlaps of the light-cone wave functions of $L_z = 0$ and $|L_z| = 1$ Fock states.

As in the case of the Pauli form factor, the generalized parton distribution (GPD) E and the Sivers function q_T involve the overlap of initial- and final-state light-front-wave-functions (LFWFS) which differ by one unit of orbital angular momentum [37]. In contrast to the Sivers function which is suppressed by one power of $(1-x)$ relative to the unpolarized distribution, one finds the GPD E falls as two-powers $(1-x)^2$ faster than the spin-conserving GPD H at large-x [38]. The power of $(1-x)^n$ thus differs when we compare the E GPD arising in spin-flip deeply virtual Compton scattering (DVCS) $\gamma^* p_\downarrow \to \gamma p_\uparrow$ and the Sivers function q_T arising in polarized electroproduction $\gamma^* p_\uparrow \to \pi X$. In the following, we will briefly comment why this happens.

It is useful to use the symmetric light-front (LF) frame where the transverse momenta of the initial and final state proton momentum changes from $\vec{p}_\perp^{\ \mathbf{initial}} = (\vec{p}_\perp - \frac{1}{2}\Delta_\perp)$ to $\vec{p}^{\ \mathbf{final}} = (\vec{p}_\perp + \frac{1}{2}\Delta_\perp)$. The struck quark in DVCS is evaluated at $\vec{k}_\perp + \frac{1}{2}(1-x)\vec{\Delta}_\perp$ in the final-state LFWF and $\vec{k}_\perp - \frac{1}{2}(1-x)\vec{\Delta}_\perp$ in the initial-state LFWF, as in the Drell-Yan-West (DYW) formula for current matrix elements [39].

The E GPD requires evaluating the spin-flip deeply virtual Compton amplitude which is linear in the transverse momentum transfer to the proton $\vec{\Delta}_\perp$. This kinematic factor arises from the extra angular momentum of the initial- or final-state LFWF with argument $\pm\frac{1}{2}(1-x)\vec{\Delta}_\perp$. In addition, the orbital angular momentum dynamics of the LFWF introduces a factor of $(1-x)$. Thus $E \sim (1-x)^2 H$ as $x \to 1$.

In contrast, when we evaluate the Sivers SSA for SIDIS $\gamma^* p \to \pi p'$, the dynamics of the orbital angular momentum in the LFWF gets expressed as the transverse momentum $\vec{p}_{\pi\perp}$ of the produced pion, not the change in the transverse momentum $\vec{\Delta}_\perp$ of the proton. Thus the second factor of $(1-x)$ does not appear in the Sivers function. We thus have the power counting rule: $E \sim (1-x) q_T \sim (1-x)^2 H$ as $x \to 1$.

E. Power counting for the integrated quark distributions at leading and higher-twist

From the power counting results for the TMD quark distributions in the last subsections, we can further derive the power counting rule for the integrated quark distributions at large-x when integrating over the transverse momentum. For example, the integrated unpolarized

quark distribution can be written as

$$q(x) = \int d^2\vec{k}_\perp q(x, k_\perp) \ . \tag{48}$$

Similar equations also hold for the longitudinal polarized quark distribution and transversity quark distribution. From the power counting of these relevant TMD quark distributions, we can immediately see that the integrated quark distributions have the following power counting rule at $x \to 1$,

$$q(x) \sim (1-x)^3, \quad \Delta q_L(x) \sim (1-x)^3, \quad \delta q_T(x) \sim (1-x)^3 \ . \tag{49}$$

To obtain the above power counting results for the integrated quark distributions, we have assumed that the $k_\perp$-integral decouples from the $x-$distributions of the partons [25, 27]. Although the upper limit of the $k_\perp$ integral might depend on $(1-x)$, the bulk of this integration comes from the lower bound, which will not affect the $(1-x)$ power counting for the integrated parton distributions [29]. The latest comparison of the above power counting predictions with experiment can be found in [40].

The $k_\perp$-moment of the $k_\perp$-odd TMD quark distributions are related to the twist-three parton distributions. For example, the twist-three parton distribution $g_T(x)$ is related to the TMD quark distribution Δg_T [30],

$$g_T(x) = \frac{1}{2xM^2} \int d^2\vec{k}_\perp \vec{k}_\perp^2 \Delta q_T(x, k_\perp) \ , \tag{50}$$

and for $h_L(x)$,

$$h_L(x) = \frac{-1}{xM^2} \int d^2\vec{k}_\perp \vec{k}_\perp^2 \delta q_L(x, k_\perp) \ . \tag{51}$$

Of course, caution has to be taken when we apply the above equations [30]. From the power counting rule for the relevant TMD quark distributions, we find the following power behavior for these two twist-three parton distributions,

$$g_T(x) \sim (1-x)^4, \quad h_L(x) \sim (1-x)^4 \ . \tag{52}$$

$k_\perp$-moment of the naive-time-reversal-odd TMD quark distributions are also related to the twist-three parton distributions, which have been shown in literature [14], for example,

$$T_F(x) = \frac{1}{M_P} \int d^2\vec{k}_\perp \vec{k}_\perp^2 q_T(x, k_\perp) \ , \tag{53}$$

where T_F is the so-called Qiu-Sterman matrix element [9], and is responsible to the SSA for inclusive hadron production in hadronic collisions. Similarly, the $k_\perp$-moment of δq corresponds,

$$T_F^{(\sigma)}(x) = \frac{1}{M_P} \int d^2\vec{k}_\perp \vec{k}_\perp^2 \delta q(x, k_\perp) \ , \tag{54}$$

where $T_F^{(\sigma)}$ is defined as

$$T_F^{(\sigma)}(x_1, x_2) = \int \frac{d\zeta^- d\eta^-}{8\pi} e^{ix_1 P^+ \eta^-} e^{i(x_2 - x_1) P^+ \zeta^-} \left\langle P|\overline{\psi}(0)\sigma^{+\alpha} g F^{+\alpha}(\zeta^-)\psi(\eta^-)|P\right\rangle \ , \tag{55}$$

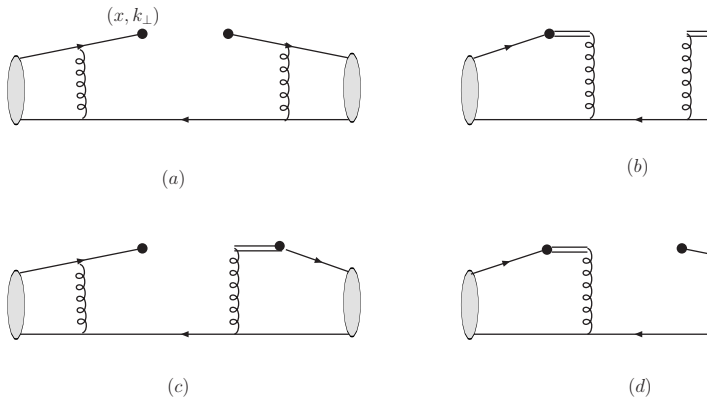

FIG. 4: *Feynman diagrams contribution to the transverse-momentum-dependent quark distribution in Pion at large-x.*

and $T_F^{(\sigma)}(x) \equiv T_F^{(\sigma)}(x,x)$. From the power counting rule of the relevant naive-time-reversal-odd TMD quark distributions, we find the power counting rule for these two twist-three parton distributions,

$$T_F(x) \sim (1-x)^4, \quad T_F^{(\sigma)}(x) \sim (1-x)^4 \ , \tag{56}$$

which are $(1-x)$ suppressed relative to the unpolarized quark distribution.

F. TMD quark distributions in Pion

A similar analysis can be carried out for the TMD quark distributions of pion. Because the pion is a spin-0 particle, there are only two leading-order TMD quark distributions: the unpolarized quark distribution $q_\pi(x, k_\perp)$ and the Boer-Mulders function $\delta q_\pi(x, k_\perp)$. At large-x, their dependence on x can be calculated from the diagrams shown in Fig. 4. The unpolarized quark distribution at large-x will have contributions from all of the four diagrams,

$$u_\pi(x, k_\perp) = \frac{f_\pi^2}{(k_\perp^2)^2}(1-x)^2\alpha_s^2 C_F \int \frac{dz_1}{z_1}\frac{dz_2}{z_2}\Phi_\pi(z_1)\Phi_\pi(z_2)\mathcal{T}_H(z_1, z_2) \ , \tag{57}$$

where f_π is the decay constant of pion, and $\Phi_\pi(z)$ is the leading-twist quark distribution amplitude. Obviously, the quark distribution has $(1-x)^2$ power behavior at large-x. This is consistent with the Gribov-Liptov relation [41].

For the Boer-Mulders function, because it is naive-time-reversal-odd, we have to take into account the interference between $L_z = 0$ and $|L_z| = 1$ Fock states of pion light-cone wave functions, and also the gauge link is important to obtain a phase difference. Following the same analysis in the previous subsections, we find that the Boer-Mulders function of pion has the same power counting result as the unpolarized quark distribution,

$$\delta q_\pi(x, k_\perp) \sim (1-x)^2 \ . \tag{58}$$

These two distribution functions having the same power behavior at large-x, is not because the Boer-Mulders function of pion gets enhancement, but because the unpolarized quark distribution of pion is suppressed by one power of $(1-x)$ compared to the usual power counting results for parton distributions of hadrons [24, 27].

III. CONCLUSION

In this paper, we have performed a perturbative analysis of the transverse momentum dependent quark distributions at large x. A generalized power counting rule has been derived for the leading order TMD quark distributions, and we have found that the $k_\perp$-even distributions all scale as $(1-x)^3$, whereas the $k_\perp$-odd ones as $(1-x)^4$, including the naive time-reversal-even and -odd distributions. In particular, we have shown that the quark Sivers function has power behavior of $(1-x)^4$, which is $(1-x)$ suppressed relative to the unpolarized quark distribution. For the TMD quark distributions of pion, we find that the Boer-Mulders function has the same power behavior as the unpolarized quark distribution, scaling as $(1-x)^2$ in the limit. These results provide important guidelines for the parameterizations of the transverse momentum dependent parton distributions and the quark-gluon correlation functions in the phenomenological studies.

In our analysis we have not included the effects of perturbative QCD evolution. In fact, the evolution of parton distributions at large x with photon virtuality Q^2 is suppressed compared to the usual DGLAP evolution [25] because the struck quark is a bound constituent of the target hadron. In particular, in the limit of $x \to 1$, the virtuality of the struck quark becomes highly space-like, and evolution is effectively quenched. Thus the power counting of structure functions at large x is not affected by evolution [25], allowing duality with the power-law falloff of exclusive channels at fixed W^2. Another important point has to be kept in mind is the large logarithms associated with the parton distributions in the $x \to 1$ limit, in terms of $\alpha_s^n \log^m(1/(1-x))$ for $m \leq 2n$ [25, 26, 42, 43]. All these effects will of course introduce additional theoretical uncertainties when we apply the power counting rule to the parton distributions at large-x.

Acknowledgments

We thank Xiangdong Ji, Jianwei Qiu, and Werner Vogelsang for their comments. S.J.B. is supported by the Department of Energy under contract number DE–AC02–76SF00515, F. Y. is grateful to RIKEN, Brookhaven National Laboratory and the U.S. Department of Energy (contract number DE-AC02-98CH10886) for providing the facilities essential for the completion of their work. Finally, F.Y. thanks Beijing Institute of Modern Physics, Institute of Theoretical Physics, Beijing University, for its warm host when part of this work was finished.

APPENDIX A: LIGHT-CONE WAVE FUNCTIONS AND DISTRIBUTION AMPLITUDES OF NUCLEON

In this Appendix we list the light-cone wave functions for the three-quark Fock states of nucleon as reference [30],

$$\begin{aligned}
|PS_{z\uparrow}\rangle &= \int d[1]d[2]d[3]\left\{\tilde{\psi}^{(1)}(1,2,3)u^\dagger_\uparrow(1)\left(u^\dagger_\downarrow(2)d^\dagger_\uparrow(3)-d^\dagger_\downarrow(2)u^\dagger_\uparrow(3)\right)|0\rangle\right. \\
&+\left((p^x_1+ip^y_1)\tilde{\psi}^{(3)}(1,2,3)+(p^x_2+ip^y_2)\tilde{\psi}^{(4)}(1,2,3)\right) \\
&\left.\left(u^\dagger_\uparrow(1)u^\dagger_\downarrow(2)d^\dagger_\downarrow(3)-d^\dagger_\uparrow(1)u^\dagger_\downarrow(2)u^\dagger_\downarrow(3)\right)|0\rangle\right\}\ , \\
|PS_{z\downarrow}\rangle &= \int d[1]d[2]d[3]\left\{-\tilde{\psi}^{(1)}(1,2,3)u^\dagger_\downarrow(1)\left(u^\dagger_\uparrow(2)d^\dagger_\downarrow(3)-d^\dagger_\uparrow(2)u^\dagger_\downarrow(3)\right)|0\rangle\right. \\
&+\left((p^x_1-ip^y_1)\tilde{\psi}^{(3)}(1,2,3)+(p^x_2-ip^y_2)\tilde{\psi}^{(4)}(1,2,3)\right) \\
&\left.\left(u^\dagger_\downarrow(1)u^\dagger_\uparrow(2)d^\dagger_\uparrow(3)-d^\dagger_\downarrow(1)u^\dagger_\uparrow(2)u^\dagger_\uparrow(3)\right)|0\rangle\right\}\ , \qquad \text{(A1)}
\end{aligned}$$

where the argument i is the shorthand for quark momentum variables y_i and $p_{i\perp}$, and the measure for the quark momentum integrations is

$$\begin{aligned}
d[1]d[2]d[3] &= \sqrt{2}\frac{dy_1dy_2dy_3}{\sqrt{2y_12y_22y_3}}\frac{d^2\vec{p}_{1\perp}d^2\vec{p}_{2\perp}d^2\vec{p}_{3\perp}}{(2\pi)^9} \\
&\times 2\pi\delta(1-y_1-y_2-y_3)(2\pi)^2\delta^{(2)}(\vec{p}_{1\perp}+\vec{p}_{2\perp}+\vec{p}_{3\perp})\ . \qquad \text{(A2)}
\end{aligned}$$

$\tilde{\psi}^{(1,3,4)}$ are the light-cone wave function amplitudes for the three quark Fock state expansion of nucleon. $\tilde{\psi}^{(1)}$ corresponds to the $L_z=0$ Fock state component, and $\tilde{\psi}^{(3,4)}$ for $|L_z|=1$ ones. These light-cone wave functions were used in our analysis for the large-x quark distributions.

In order to get Eq. (3), the light-cone wave functions have to be converted into the quark distribution amplitudes [25]. For example, we can integrate out the transverse momentum in the leading Fock state light-cone wave function, and define the twist-three amplitude,

$$\Phi_3(y_i)=2\sqrt{6}\int\frac{d^2\vec{p}_{1\perp}d^2\vec{p}_{2\perp}d^2\vec{p}_{3\perp}}{(2\pi)^6}\delta^{(2)}(\vec{p}_{1\perp}+\vec{p}_{2\perp}+\vec{p}_{3\perp})\tilde{\psi}^{(1)}(1,2,3)\ . \qquad \text{(A3)}$$

For $|L_z|=1$ states, we have to keep linear term in the $p_\perp$ expansion of the hard factor, and combine them with the light-cone wave function, which will lead to the twist-four distribution amplitudes of the nucleon [44, 45],

$$\begin{aligned}
\Psi_4(y_1,y_2,y_3) &= \frac{2\sqrt{6}}{y_2M}\int\frac{d^2\vec{p}_{1\perp}d^2\vec{p}_{2\perp}d^2\vec{p}_{3\perp}}{(2\pi)^6}\delta^{(2)}(\vec{p}_{1\perp}+\vec{p}_{2\perp}+\vec{p}_{3\perp}) \\
&\times\vec{p}_{2\perp}\cdot\left[\vec{p}_{1\perp}\tilde{\psi}^{(3)}(1,2,3)+\vec{p}_{2\perp}\tilde{\psi}^{(4)}(1,2,3)\right]\ . \\
\Phi_4(y_2,y_1,y_3) &= \frac{2\sqrt{6}}{y_3M}\int\frac{d^2\vec{p}_{1\perp}d^2\vec{p}_{2\perp}d^2\vec{p}_{3\perp}}{(2\pi)^6}\delta^{(2)}(\vec{p}_{1\perp}+\vec{p}_{2\perp}+\vec{p}_{3\perp}) \\
&\times\vec{p}_{3\perp}\cdot\left[\vec{p}_{1\perp}\tilde{\psi}^{(3)}(1,2,3)+\vec{p}_{2\perp}\tilde{\psi}^{(4)}(1,2,3)\right]\ . \qquad \text{(A4)}
\end{aligned}$$

The explicit expressions for these distribution amplitudes are not necessary for the power-counting analysis. However, the end-point behavior at $y_i \to 1$ is needed for the power counting of the naive time-reversal-odd TMD quark distributions. We note that in the end-point region, these distribution amplitudes have the following behaviors: $\Phi_3(y_i) \propto y_1 y_2 y_3$, $y_2\Psi_4(y_i) \propto y_1 y_2 y_3$, and $y_3\Phi_4(y_i) \propto y_1 y_2 y_3$ [44]. From this, we immediately find that the end-point behavior of the $p_\perp$-moment of the light-cone wave functions. For example,

$$\int d^2\vec{p}_{1\perp} d^2\vec{p}_{2\perp} d^2\vec{p}_{3\perp} \delta^{(2)}(\vec{p}_{1\perp} + \vec{p}_{2\perp} + \vec{p}_{3\perp})(\vec{p}_{i\perp} \cdot \vec{p}_{j\perp}) \tilde{\psi}^{(3,4)}(y_1, y_2, y_3)|_{\text{end point}} \sim y_1 y_2 y_3 \ , \quad \text{(A5)}$$

where $i, j = 1, 2, 3$. These properties have been used in our analysis.

---

[1] see for example: G. Bunce *et al.*, Phys. Rev. Lett. **36**, 1113 (1976); D. L. Adams *et al.* [E581 and E704 Collaborations], Phys. Lett. B **261**, 201 (1991); D. L. Adams *et al.* [FNAL-E704 Collaboration], Phys. Lett. B **264**, 462 (1991); K. Krueger *et al.*, Phys. Lett. B **459**, 412 (1999).

[2] A. Airapetian *et al.* [HERMES Collaboration], Phys. Rev. Lett. **84**, 4047 (2000); A. Airapetian *et al.* [HERMES Collaboration], Phys. Rev. D **64**, 097101 (2001); Phys. Rev. Lett. **94**, 012002 (2005); M. Diefenthaler [HERMES Collaboration], arXiv:hep-ex/0507013.

[3] V. Y. Alexakhin *et al.* [COMPASS Collaboration], Phys. Rev. Lett. **94**, 202002 (2005).

[4] H. Avakian *et al.* [CLAS Collaboration], Phys. Rev. D **69**, 112004 (2004) [arXiv:hep-ex/0301005]; H. Avakian, P. Bosted, V. Burkert and L. Elouadrhiri [CLAS Collaboration], AIP Conf. Proc. **792**, 945 (2005) [arXiv:nucl-ex/0509032].

[5] J. Adams *et al.* [STAR Collaboration], Phys. Rev. Lett. **92**, 171801 (2004) [arXiv:hep-ex/0310058].

[6] S. S. Adler [PHENIX Collaboration], Phys. Rev. Lett. **95**, 202001 (2005) [arXiv:hep-ex/0507073].

[7] F. Videbaek [BRAHMS Collaboration], AIP Conf. Proc. **792**, 993 (2005); arXiv:nucl-ex/0601008. J. H. Lee [BRAHMS Collaboration], talk presented at the "14th International Workshop on Deep Inelastic Scattering (DIS 2006)", Tsukuba, Japan, April 20-24, 2006.

[8] A. V. Efremov and O. V. Teryaev, Sov. J. Nucl. Phys. **36**, 140 (1982) [Yad. Fiz. **36**, 242 (1982)]; A. V. Efremov and O. V. Teryaev, Phys. Lett. B **150**, 383 (1985).

[9] J.W. Qiu and G. Sterman, Phys. Rev. Lett. **67**, 2264 (1991); Nucl. Phys. B **378**, 52 (1992); Phys. Rev. D **59**, 014004 (1999).

[10] D. W. Sivers, Phys. Rev. D **41**, 83 (1990); Phys. Rev. D **43**, 261 (1991).

[11] S. J. Brodsky, D. S. Hwang and I. Schmidt, Phys. Lett. B **530**, 99 (2002); Nucl. Phys. B **642**, 344 (2002).

[12] J. C. Collins, Phys. Lett. B **536**, 43 (2002).

[13] X. Ji and F. Yuan, Phys. Lett. B **543**, 66 (2002); A. V. Belitsky, X. Ji and F. Yuan, Nucl. Phys. B **656**, 165 (2003).

[14] D. Boer, P. J. Mulders and F. Pijlman, Nucl. Phys. B **667**, 201 (2003).

[15] J. C. Collins and D. E. Soper, Nucl. Phys. B **193**, 381 (1981) [Erratum-ibid. B **213**, 545 (1983)]; Nucl. Phys. B **197**, 446 (1982); J. C. Collins and D. E. Soper, Nucl. Phys. B **194**, 445 (1982).

[16] J. C. Collins, D. E. Soper and G. Sterman, Nucl. Phys. B **250**, 199 (1985).

[17] X. Ji, J. P. Ma and F. Yuan, Phys. Rev. D **71**, 034005 (2005); Phys. Lett. B **597**, 299 (2004); JHEP **0507**, 020 (2005) [arXiv:hep-ph/0503015].
[18] J. C. Collins and A. Metz, Phys. Rev. Lett. **93**, 252001 (2004).
[19] X. Ji, J. W. Qiu, W. Vogelsang and F. Yuan, Phys. Rev. Lett. **97**, 082002 (2006) [arXiv:hep-ph/0602239]; Phys. Rev. D **73**, 094017 (2006) [arXiv:hep-ph/0604023]; Phys. Lett. B **638**, 178 (2006) [arXiv:hep-ph/0604128].
[20] M. Anselmino, M. Boglione, U. D'Alesio, A. Kotzinian, F. Murgia and A. Prokudin, Phys. Rev. D **72**, 094007 (2005) [Erratum-ibid. D **72**, 099903 (2005)] [arXiv:hep-ph/0507181]; Phys. Rev. D **71**, 074006 (2005) [arXiv:hep-ph/0501196].
[21] W. Vogelsang and F. Yuan, Phys. Rev. D **72**, 054028 (2005) [arXiv:hep-ph/0507266].
[22] J. C. Collins, A. V. Efremov, K. Goeke, S. Menzel, A. Metz and P. Schweitzer, Phys. Rev. D **73**, 014021 (2006) [arXiv:hep-ph/0509076]; J. C. Collins *et al.*, Phys. Rev. D **73**, 094023 (2006) [arXiv:hep-ph/0511272].
[23] C. Kouvaris, J. W. Qiu, W. Vogelsang and F. Yuan, arXiv:hep-ph/0609238.
[24] G. R. Farrar and D. R. Jackson, Phys. Rev. Lett. **35**, 1416 (1975).
[25] G. P. Lepage and S. J. Brodsky, Phys. Rev. D **22**, 2157 (1980).
[26] A. H. Mueller, Phys. Rept. **73**, 237 (1981).
[27] J. F. Gunion, P. Nason and R. Blankenbecler, Phys. Rev. D **29**, 2491 (1984).
[28] S. J. Brodsky, M. Burkardt and I. Schmidt, Nucl. Phys. B **441**, 197 (1995) [arXiv:hep-ph/9401328].
[29] X. Ji, J. P. Ma and F. Yuan, Phys. Lett. B **610**, 247 (2005) [arXiv:hep-ph/0411382].
[30] X. Ji, J. P. Ma and F. Yuan, Nucl. Phys. B **652**, 383 (2003) [arXiv:hep-ph/0210430].
[31] S. J. Brodsky and S. Gardner, arXiv:hep-ph/0608219.
[32] S. J. Brodsky and S. D. Drell, Phys. Rev. D **22**, 2236 (1980).
[33] P. J. Mulders and R. D. Tangerman, Nucl. Phys. B **461**, 197 (1996) [Erratum-ibid. B **484**, 538 (1997)] [arXiv:hep-ph/9510301]; D. Boer and P. J. Mulders, Phys. Rev. D **57**, 5780 (1998) [arXiv:hep-ph/9711485].
[34] R. L. Jaffe and X. Ji, Nucl. Phys. B **375**, 527 (1992).
[35] J. C. Collins, Nucl. Phys. B **396**, 161 (1993) [arXiv:hep-ph/9208213].
[36] J. Soffer, Phys. Rev. Lett. **74**, 1292 (1995) [arXiv:hep-ph/9409254].
[37] S. J. Brodsky, M. Diehl and D. S. Hwang, Nucl. Phys. B **596**, 99 (2001) [arXiv:hep-ph/0009254].
[38] F. Yuan, Phys. Rev. D **69**, 051501 (2004) [arXiv:hep-ph/0311288].
[39] S. D. Drell and T. M. Yan, Phys. Rev. Lett. **24**, 855 (1970); G. B. West, Phys. Rev. Lett. **24**, 1206 (1970).
[40] X. Zheng *et al.* [Jefferson Lab Hall A Collaboration], Phys. Rev. Lett. **92**, 012004 (2004) [arXiv:nucl-ex/0308011]; Phys. Rev. C **70**, 065207 (2004) [arXiv:nucl-ex/0405006].
[41] V. N. Gribov and L. N. Lipatov, Sov. J. Nucl. Phys. **15**, 675 (1972) [Yad. Fiz. **15**, 1218 (1972)].
[42] G. P. Korchemsky, Mod. Phys. Lett. A **4**, 1257 (1989).
[43] G. Sterman, Nucl. Phys. B **281**, 310 (1987).
[44] V. Braun, R. J. Fries, N. Mahnke and E. Stein, Nucl. Phys. B **589**, 381 (2000) [Erratum-ibid. B **607**, 433 (2001)] [arXiv:hep-ph/0007279].
[45] A. V. Belitsky, X. Ji and F. Yuan, Phys. Rev. Lett. **91**, 092003 (2003) [arXiv:hep-ph/0212351].